

Projected Data Assimilation

John Maclean* and Erik S Van Vleck†

Abstract. We introduce a framework for Data Assimilation (DA) in which the data is split into multiple sets corresponding to low-rank projections of the state space. Algorithms are developed that assimilate some or all of the projected data, including an algorithm compatible with any generic DA method. The major application explored here is PF-AUS, a new implementation of Assimilation in the Unstable Subspace (AUS) for Particle Filters. The PF-AUS implementation assimilates highly informative but low-dimensional observations. In the context of particle filtering, the projected approach mitigates the collapse of particle ensembles in high dimensional DA problems while preserving as much relevant information as possible, as the unstable and neutral modes correspond to the most uncertain model predictions. In particular we formulate and numerically implement PF-AUS with the optimal proposal and compare to the standard optimal proposal and to the Local Ensemble Transform Kalman Filter.

Key words. Data Assimilation, Numerical Analysis, Dimension Reduction

AMS subject classifications. 93E11, 93C10, 93B17, 60G35

1. Introduction. Many Bayesian data assimilation techniques were developed based on extending assumptions of linearity in the phase space and data models and under the assumption of Gaussian errors. Several techniques have proven to be successful in weakening these assumptions, while other techniques have been developed to explicitly overcome these obstacles. Important among these are particle filters, a key subject of this paper. Particle filters have proven to be successful for low dimensional problems but tend to have difficulty with higher dimensional problems. Different variants of particle filters have been developed to combat these difficulties, including implicit particle filters, the optimal proposal, proposal density methods, etc..

Our contribution in this paper is to develop a framework for data assimilation schemes in which the data are constrained by a projection to lie in some subspace of observation or model space. This is motivated in large part by assimilation in the unstable subspace (AUS) techniques. These techniques have largely focused on projecting the phase space model using Lyapunov vectors while employing the original data or observational model. The techniques and framework developed in this paper allow for combinations of projected and unprojected physical and data models and their formulation is independent of the source of the time dependent projections. Using the framework developed here, we focus on techniques for projecting the observations in particle filters to lessen the impact of the curse of dimensionality. The

*School of Mathematical Sciences, University of Adelaide, South Australia. <http://www.adelaide.edu.au/directory/john.maclean>

†Department of Mathematics, University of Kansas, USA. <https://mathematics.ku.edu/erik-van-vleck>

framework and techniques lead to several natural applications. In particular we develop, implement, and compare two new particle filter algorithms based upon a dimension reduction technique into the unstable subspace and to show the application of these projected particle filter techniques.

The approach is related to three past approaches that use projections to identify a low-dimensional subspace that captures the most uncertain, or most nonlinear, directions in state space. The AUS techniques [7, 36, 16, 26, 19, 29] to improve speed and reliability of data assimilation specifically address the partitioning of the tangent space into stable, neutral and unstable subspaces corresponding to Lyapunov vectors associated with negative, zero and positive Lyapunov exponents. In particular, Trevisan, d'Isidoro & Talagrand propose a modification of 4DVar, so-called 4DVar-AUS, in which corrections are applied only in the unstable and neutral subspaces [36, 26]. These techniques are based on updating in the unstable portion of the tangent space and may be interpreted in terms of projecting covariance matrices during the assimilation step.

Motivated by these techniques for assimilation in the unstable subspace, in [8] a new method is developed for data assimilation that utilizes distinct treatments of the dynamics in the stable and non-stable directions. In particular, the first phase of this development has involved employing time dependent Lyapunov vectors to form a subsystem with tangent space dynamics similar to the unstable subspace of the original state space model. This is motivated by the AUS techniques (e.g. [7, 36]). In [8] the following Newton like iteration was considered, alternatively correcting in the unstable space and the stable subspace. For a smooth discrete time model $u_{n+1} = F_n(u_n)$ and projection \mathbf{P}_n , alternate solving the two projected subsystems, using shadowing refinement in the first subsystem and forward in time evolution in the second. Here k is the Newton iterate. With $\{u_n^{(k)}\}_{n=0}^N$ known, solve for $\{d_n\}_{n=0}^N$, $d_n := \mathbf{P}_n \delta_n$, and then update:

$$(1.1) \quad u_{n+1}^{(k)} + d_{n+1} = \mathbf{P}_{n+1} F_n(u_n^{(k)} + d_n), \quad u_n^{(k+\frac{1}{2})} = u_n^{(k)} + d_n, \quad n = 0, 1, \dots, N-1.$$

For the $\{u_n^{(k+\frac{1}{2})}\}_{n=0}^N$ known, solve for $\{e_n\}_{n=0}^N$, $e_n := (\mathbf{I} - \mathbf{P}_n) \delta_n$, and update:

$$(1.2) \quad u_{n+1}^{(k+\frac{1}{2})} + e_{n+1} = (\mathbf{I} - \mathbf{P}_{n+1}) F_n(u_n^{(k+\frac{1}{2})} + e_n), \quad u_n^{(k+1)} = u_n^{(k+\frac{1}{2})} + e_n, \quad n = 0, 1, \dots, N-1.$$

This manuscript develops a complementary approach to project the data model as well.

The third branch of projected DA schemes use the ‘Dynamically Orthogonal’ (DO) formulation [31, 30], in which the forecast model is broken into a partial differential equation governing the mean field and a number of stochastic differential equations describing the evolution of components in a time-dependent stochastic subspace of the original differential equation. The DO approach was used to assimilate with different DA schemes in the subspace and mean field space in [35, 23, 27].

We develop a projected DA framework and algorithms for arbitrary time dependent orthogonal projections, but are mainly interested in the AUS approach where the projections identify the unstable/neutral subspace. To determine the projections we will employ standard techniques

for approximation of Lyapunov exponents, e.g., the so-called discrete QR algorithm (see [9, 10]). Unlike past work on the topic we will focus on confining the data, not the model, to the unstable subspace. If the non-stable subspace is relatively low dimensional this makes applications of techniques such as particle filters appealing.

Particle Filters [11] are particularly effective for nonlinear problems and for the tracking of non-Gaussian, multi-modal probability distributions; but they suffer from the so-called curse of dimensionality (see, e.g., Snyder [33, 32] Morzfeld et al. [25] and Van Leeuwen [39]). There is a known formulation that minimises degeneracy; however, even with a linear model, it is known that the computational cost of this "Optimal Proposal" Particle Filter scales like the exponential of the observation dimension [32]. Our aim in this work is to avoid the established limits of particle filter performance by reducing the observation dimension in a sensible way. Other efforts to bypass this limitation include, e.g., the Equivalent Weights Particle Filter [40]. One attractive feature of our approach is that it is a reformulation of the standard DA problem rather than a specific algorithm, and so it is compatible with these advanced particle filters.

The availability of the projection into the unstable subspace will also allow us to develop a novel approach to resampling. It is necessary to periodically refresh any particle ensemble, and some noise is usually added at this step. To avoid forcing the ensemble off the attractor with this added noise we confine most of the noise to the unstable subspace, which improves the filter accuracy and reduces the incidence of resampling in later steps.

This paper is organized as follows. Data assimilation is reviewed in section 2 and projected DA is formulated in section 3. Algorithms for using the new projected data are introduced (section 4) and applied to AUS with several numerical experiments (section 5). A discussion (section 6) and bibliography conclude the paper.

2. Data Assimilation. Data assimilation methods combine orbits from a dynamical system model with measurement data to obtain an improved estimate for the state of a physical system. In this paper we develop a data assimilation method in the context of the discrete time stochastic model

$$(2.1) \quad u_{n+1} = F_n(u_n) + \omega_n, \quad n = 0, 1, \dots$$

where $u_n \in \mathbb{R}^N$ are the state variables at time n and $\omega_n \sim \mathcal{N}(0, \Sigma)$, i.e., drawn from a normal distribution with mean zero and model error covariance Σ . Let the sequence $\{u_0^t, u_1^t, \dots\}$, be a distinguished orbit of this system, referred to as the *true solution* of the model, and presumed to be unknown. As each time t_n is reached we collect an observation y_n related to u_n^t via

$$(2.2) \quad y_n = \mathbf{H}u_n^t + \eta_n, \quad y_n \in \mathbb{R}^M$$

where $\mathbf{H} : \mathbb{R}^N \rightarrow \mathbb{R}^M$, $M \leq N$, is the observation operator, and the noise variables η_n are drawn from a normal distribution $\eta_n \sim \mathcal{N}(0, \mathbf{R})$ with zero mean and known observational error covariance matrix \mathbf{R} . In general the observation operator can be nonlinear.

We formulate DA under the ubiquitous Bayesian approach. Consider the assimilation of a

single observation, y_n , at time step n . Given a prior estimate $p(u_n)$ of the state, Bayes' Law gives

$$p(u_n|y_n) \propto p(y_n|u_n)p(u_n),$$

Using (2.2) the likelihood function is, up to a normalization constant,

$$(2.3) \quad p(y_n|u_n) \propto \exp \left[(y_n - \mathbf{H}u_n)^T \mathbf{R}^{-1} (y_n - \mathbf{H}u_n) \right].$$

This procedure, which we have written for the assimilation of data at a single observation time, readily extends to the sequential assimilation of observations at multiple times under the assumptions that the state is Markovian and the observations at different times are conditionally independent (see for example [4]).

In the following we introduce some key DA schemes. Not much detail is given here, but the interested reader is referred in particular to three recent books on DA, [28, 20, 1].

2.1. Kalman Filtering. The Kalman Filter and later extensions are ubiquitous in DA, and are now briefly described. For a linear model, i.e. where (2.1) is

$$(2.4) \quad u_{n+1} = \mathbf{A}_n u_n + \omega_n,$$

and for the linear observation operator \mathbf{H} , the Kalman Filter calculates the exact posterior $u_n|y_n \sim \mathcal{N}(u_n^a, P_n^a)$, where the *analysis* variables are

$$(2.5) \quad u_n^a = u_n^f + \mathbf{K}_n (y_n - \mathbf{H}u_n^f),$$

$$(2.6) \quad P_n^a = (\mathbf{I} - \mathbf{K}_n \mathbf{H}) P_n^f.$$

The weight matrix \mathbf{K}_n is the Kalman gain matrix

$$(2.7) \quad \mathbf{K}_n = P_n^f \mathbf{H}^T \left(\mathbf{H} P_n^f \mathbf{H}^T + \mathbf{R} \right)^{-1}.$$

The superscript f is reserved for *forecast* variables, obtained at time n by using (2.4) to update $\{u_{n-1}^a, P_{n-1}^a\}$,

$$u_n^f = \mathbf{A}_{n-1} u_{n-1}^a + \omega_{n-1},$$

$$P_n^f = \mathbf{A}_{n-1} P_{n-1}^a \mathbf{A}_{n-1}^T + \Sigma.$$

The covariance matrices P_n^f and P_n^a are not bolded in order to distinguish them from the projections \mathbf{P}_n that are the focus of the remainder of the paper. Two extensions of the Kalman Filter are prevalent in nonlinear DA, the Extended Kalman Filter (EKF) and Ensemble Kalman Filter (EnKF). Neither give the exact posterior for a nonlinear model.

2.1.1. Extended Kalman Filter. The nonlinear model (2.1) is used to make the forecast u_n^f , and then the Kalman Filter update is applied using the linearisation

$$\mathbf{A}_n = \frac{\partial F_n}{\partial u} \Big|_{u_{n-1}^a} .$$

If the observation operator is a nonlinear function $h()$, the linearization

$$\mathbf{H}_n = \frac{dh}{du} \Big|_{u_n^f}$$

is used everywhere except to compute the *innovation* $y_n - h(u_n^f)$ in the calculation of y_n^a . The EKF is suitable for low dimensional nonlinear filtering, but the required linearizations are nontrivial for high-dimensional filtering. The EnKF by contrast is well suited to high dimensions.

2.1.2. Ensemble Kalman Filter. The Ensemble Kalman Filter is a Monte Carlo approximation of the Kalman Filter that is well suited to high dimensional filtering problems, introduced in [13, 5]. An ensemble of forecasts $u_n^{f,i}$ are made at time t_n , i from 1 to L . Then the forecast covariance P_n^f is approximated by the sample covariance of the ensemble, and the analysis ensemble $u_n^{a,i}$ is obtained in such a way that its mean $\bar{x}_n^a = \frac{1}{L} \sum_i u_n^{a,i}$ satisfies (2.5) and its sample covariance satisfies (2.6). In this paper we will use analysis updates corresponding to the Ensemble Transform Kalman Filter (ETKF) [2] or Local Ensemble Transform Filter (LETKF) [17]. For more details and a modern introduction to the Ensemble Kalman Filter, see e.g. [14].

2.2. The Particle Filter. Particle Filters (PF) are a collection of particle based data assimilation schemes do not rely on linearization of the dynamics or Gaussian representations of the posterior; see [11] for a comprehensive review. The basic idea is to represent the prior distribution $p(u_n)$, previously the forecast, and the posterior distribution $p(u_n|y_n)$, previously the analysis, by discrete probability measures. Suppose that at time $n-1$ we have the posterior distribution (u_{n-1}^i, w_{n-1}^i) , supported on points $u_{n-1}^1, \dots, u_{n-1}^L$ and with weights $w_{n-1}^1, \dots, w_{n-1}^L$. Each $w_{n-1}^i \geq 0$ and $\sum_{i=1}^L w_{n-1}^i = 1$. Here L is the number of particles that are used to approximate the distribution Π_{n-1} . The two key steps in the Particle Filter are as follows:

Prediction step. Propagate each of the particles $u_{n-1}^i \mapsto u_n^i$. One simple choice, the bootstrap PF, is to use the state dynamics (2.1) to forecast each particle.

This gives the forecast probability distribution as a discrete probability measure concentrated on L points $\{u_n^i\}_{i=1}^L$ with weights $\{w_{n-1}^i\}_{i=1}^L$.

Filtering step. Update the weights $\{w_{n-1}^i\}_{i=1}^L$ using the observation y_n by setting

$$w_n^i = c w_{n-1}^i p(y_n|u_n^i),$$

where c is chosen so that $\sum_{i=1}^L w_n^i = 1$.

This scheme is easy to implement but suffers from severe degeneracy, especially in high dimensions. That is, after a few time steps all the weight tends to concentrate on a few particles. A common remedy is to monitor the Effective Sample Size (ESS) and resample when the ESS drops below some threshold in order to refresh the particle cloud; see e.g. [11, 4].

2.2.1. The Optimal Proposal. The optimal proposal particle filter (OP-PF) [33, 12, 32, 39] attempts to address the degeneracy issue in particle filters with the aim of ensuring that all posterior particles have similar weights. The ‘proposal’ is the distribution used to update the particles from one time step to the next. In the prediction step in the basic particle filter above, the particles are updated using the model, so the proposal density in that approach is (compare (2.1)) $p(u_n^i|u_{n-1}^i) \sim \mathcal{N}(F_{n-1}(u_{n-1}^i), \Sigma)$.

The optimal proposal density is $p(u_n^i|u_{n-1}^i, y_n)$. Given the additive noise of the model (2.1), the optimal proposal update in each particle is Gaussian with $p(u_n^i|u_{n-1}^i, y_n) \sim \mathcal{N}(m_n^i, \Sigma_p)$, where

$$(2.8) \quad \Sigma_p^{-1} = \Sigma^{-1} + \mathbf{H}^T \mathbf{R}^{-1} \mathbf{H},$$

$$(2.9) \quad m_n = F_{n-1}(u_{n-1}) + \Sigma_p \mathbf{H}^T \mathbf{R}^{-1} (y_n - \mathbf{H} F_{n-1}(u_{n-1})).$$

The prefactor $\Sigma_p \mathbf{H}^T \mathbf{R}^{-1}$ can be written as the Kalman gain (2.7) (albeit with $P_n^f = \Sigma$) by an application of the Sherman-Morrison-Woodbury formula (see e.g. [18], p. 171).

Two applications of Bayes’ law (e.g. in [32]) show that the weight update for the i -th particle drawn from this proposal satisfies $w_n^i \propto p(y_n|u_{n-1}^i) w_{n-1}^i$ and is also Gaussian,

$$(2.10) \quad p(y_n|u_{n-1}) \propto \exp \left[-\frac{1}{2} (y_n - \mathbf{H} F_{n-1}(u_{n-1}))^T (\Sigma + \mathbf{H}^T \mathbf{R} \mathbf{H})^{-1} (y_n - \mathbf{H} F_{n-1}(u_{n-1})) \right].$$

As mentioned in the previous section, degeneracy - characterised by a single particle with weight of approximately 1 - is a common problem in the PF. In [34] it is shown that, of all PF schemes that obtain u_n^i using u_{n-1}^i and y_n , the ‘optimal proposal’ above has the minimum variance in the weights. That is, it suffers the least from weight degeneracy. In [41] this result is extended to any PF scheme that obtains u_n^i using i , $u_{n-1}^{1:L}$ and y_n .

The distributions required to apply the Optimal Proposal are not always available (the additive model error of (2.1) and linear observation operator of (2.2) are required above to ensure the Gaussian character of the individual particle updates and weight updates), but when OP-PF can be formulated it is the least degenerate of a large class of filters. However, in [32] it is shown that the optimal proposal requires an ensemble size L satisfying $\log L \propto N \times M$ for a linear model, or will suffer from filter degeneracy.

That is, filter degeneracy is intimately connected to model and observation dimension, and is a fundamental component of most Particle Filters.

3. Formulating projected DA. We are developing techniques that decompose the state space model and observational model based upon the time dependent stability properties of the state space model. Suppose that at time n a dynamically significant rank p orthogonal

projection $\mathbf{P}_n \in \mathbb{R}^{N \times N}$ is available, along with a splitting $\mathbf{P}_n = \mathbf{Q}_n \mathbf{Q}_n^T$, where $\mathbf{Q}_n \in \mathbb{R}^{N \times p}$ has orthonormal columns. In the application motivated above the projection identifies unstable modes, but the derivation below does not require this interpretation of \mathbf{P}_n .

The main result will be to derive a new data model

$$(3.1) \quad y_n^q = \tilde{\mathbf{Q}}_n^T \mathbf{P}_n u_n^t + \gamma_n$$

that is a linear transformation of (2.2), where $\tilde{\mathbf{Q}}_n$ is derived from \mathbf{Q}_n , \mathbf{P}_n from \mathbf{H} , and γ_n has known distribution. This new data model assimilates only the components of observations that can be written as a linear combination of the columns of \mathbf{Q}_n .

We will derive (3.1) in three steps. The first obstacle to be overcome is that the projection \mathbf{P}_n is in state space with $\mathbf{P}_n \in \mathbb{R}^{N \times N}$, while $y_n \in \mathbb{R}^M$ typically has different dimension.

3.1. Observations as a subspace of model space. Assume that \mathbf{H} has full row rank. Then defining $\tilde{y}_n = \mathbf{H}^\dagger y_n$ where $\mathbf{H}^\dagger = \mathbf{H}^T (\mathbf{H}\mathbf{H}^T)^{-1}$, and defining $\mathbf{P}_\mathbf{H} = \mathbf{H}^\dagger \mathbf{H}$, the data model for \tilde{y}_n is

$$\begin{aligned} \tilde{y}_n &= \mathbf{H}^\dagger y_n \\ &= \mathbf{P}_\mathbf{H} u_n^t + \mathbf{H}^\dagger \eta_n \\ &= \mathbf{P}_\mathbf{H} u_n^t + \psi_n \end{aligned}$$

where $\psi_n \sim \mathcal{N}(0, \mathbf{H}^\dagger \mathbf{R} (\mathbf{H}^\dagger)^T)$.

The covariance matrix $\mathbf{H}^\dagger \mathbf{R} (\mathbf{H}^\dagger)^T$ is positive semi-definite and \tilde{y}_n has a singular normal distribution [38]. Using that $\mathbf{H}\mathbf{H}^\dagger = \mathbf{I}$ one readily confirms that $\mathbf{H}\tilde{y}_n = y_n = \mathbf{H}u_n^t + \eta_n$, that is the observation operator collapses \tilde{y}_n onto the standard data model. The transformation through \mathbf{H}^\dagger has not affected the output of a DA scheme, as $p(\tilde{y}_n|x) = p(y_n|x)$.

3.2. Using the projections. We now make use of the orthogonal projection $\mathbf{P}_n = \mathbf{Q}_n \mathbf{Q}_n^T$. The idea is to formulate a new data model, along the lines of $\mathbf{P}_n \tilde{y}_n = \mathbf{P}_n \mathbf{P}_\mathbf{H} u_n^t + \mathbf{P}_n \mathbf{H}^\dagger \eta_n$, that contains only the components of the observation that align with the projection.

Depending on the dimension of the observations and on the rank of the projection p , there are two ways this might be achieved. One way, as above, is to directly apply the projection \mathbf{P}_n to \tilde{y} . The product of projections $\mathbf{P}_n \mathbf{P}_\mathbf{H}$ that is applied to the state vector in this data model is not itself a projection; in some circumstances it might be desired to instead identify the projection $\mathbf{P}_n^\mathbf{H}$ that is the intersection of \mathbf{P}_n and $\mathbf{P}_\mathbf{H}$. This projection $\mathbf{P}_n^\mathbf{H}$ may be approximated accurately by e.g. Von Neumann's algorithm or Dykstra's projection algorithm; see Appendix A for a review. The construction of $\mathbf{P}_n^\mathbf{H}$ is possible in only some assimilation problems, in particular those in which the transversality condition $p + M - N > 0$ is satisfied; otherwise there is no guarantee of any intersection between \mathbf{P}_n and $\mathbf{P}_\mathbf{H}$.

For convenience we denote by $\tilde{\mathbf{P}}_n$ either \mathbf{P}_n if $p + M - N \leq 0$, or \mathbf{P}_n^H if $p + M - N > 0$, and denote by $\tilde{\mathbf{Q}}_n$ the matrix with orthonormal columns satisfying $\tilde{\mathbf{P}}_n = \tilde{\mathbf{Q}}_n \tilde{\mathbf{Q}}_n^T$. This matrix is already known from the QR decomposition (5.1) if $\tilde{\mathbf{P}}_n = \mathbf{P}_n$, or can be calculated via the singular value or Schur decomposition if $\tilde{\mathbf{P}}_n = \mathbf{P}_n^H$. For the case $\tilde{\mathbf{P}}_n = \mathbf{P}_n^H$ we abuse notation by redefining p as the rank of $\tilde{\mathbf{P}}_n$.

Define $y_n^p = \tilde{\mathbf{P}}_n \tilde{y}_n = \tilde{\mathbf{P}}_n \mathbf{H}^\dagger y_n \in \mathbb{R}^N$, the projected observation. The data model is

$$\begin{aligned} y_n^p &= \tilde{\mathbf{P}}_n \mathbf{H}^\dagger y_n \\ &= \tilde{\mathbf{P}}_n \mathbf{P}_H u_n^t + \tilde{\mathbf{P}}_n \mathbf{H}^\dagger \eta_n \\ (3.2) \quad &= \tilde{\mathbf{P}}_n u_n^t + \xi_n \end{aligned}$$

where $\xi_n \sim \mathcal{N}(0, \tilde{\mathbf{P}}_n \mathbf{H}^\dagger \mathbf{R}(\mathbf{H}^\dagger)^T \tilde{\mathbf{P}}_n)$. The data model y_n^p has a singular normal distribution with support in the p -dimensional subspace of model space spanned by the columns of $\tilde{\mathbf{Q}}_n$, and the likelihood of this distribution can be written using the pseudo-inverse (see e.g. [38]) as

$$(3.3) \quad p(y_n^p | u) \propto \exp \left(-\frac{1}{2} \left(y_n^p - \tilde{\mathbf{P}}_n \mathbf{P}_H u \right)^T \left(\tilde{\mathbf{P}}_n \mathbf{H}^\dagger \mathbf{R}(\mathbf{H}^\dagger)^T \tilde{\mathbf{P}}_n \right)^\dagger \left(y_n^p - \tilde{\mathbf{P}}_n \mathbf{P}_H u \right) \right) .$$

Remark 1. If $\tilde{\mathbf{P}}_n$ is invertible then the distribution of y_n^p is non-singular, $p(y_n^p | u) = p(y_n | u)$, and the above construction does not affect the output of a DA scheme.

To make explicit the reduction in the data dimension that has been obtained by y_n^p we introduce a low dimensional data model $y_n^q = \tilde{\mathbf{Q}}_n^T \tilde{y}_n \in \mathbb{R}^p$. The following result establishes that y_n^q is equivalent to (3.2).

Theorem 3.1. Define $y_n^q = \tilde{\mathbf{Q}}_n^T \tilde{y}_n$, with the associated data model

$$(3.4) \quad y_n^q = \mathbf{H}_n^q u_n^t + \gamma_n ,$$

where $\mathbf{H}_n^q = \tilde{\mathbf{Q}}_n^T \mathbf{P}_H$, $\gamma_n \sim \mathcal{N}(0, \mathbf{R}_n^q)$, and $\mathbf{R}_n^q = \tilde{\mathbf{Q}}_n^T \mathbf{H}^\dagger \mathbf{R}(\mathbf{H}^\dagger)^T \tilde{\mathbf{Q}}_n$. Then $p(y_n^q | u) = p(y_n^p | u)$.

Proof. The matrix $\tilde{\mathbf{Q}}_n$ has orthonormal columns so $\tilde{\mathbf{Q}}_n^\dagger = \tilde{\mathbf{Q}}_n^T$ and for any matrix \mathbf{B}

$$\begin{aligned} \left(\tilde{\mathbf{Q}}_n \mathbf{B} \right)^\dagger &= \mathbf{B}^\dagger \tilde{\mathbf{Q}}_n^\dagger = \mathbf{B}^\dagger \tilde{\mathbf{Q}}_n^T , \\ \left(\mathbf{B} \tilde{\mathbf{Q}}_n^T \right)^\dagger &= (\tilde{\mathbf{Q}}_n^T)^\dagger \mathbf{B}^\dagger = \tilde{\mathbf{Q}}_n \mathbf{B}^\dagger . \end{aligned}$$

Applying these results to (3.3), and using that $\tilde{\mathbf{P}}_n = \tilde{\mathbf{Q}}_n \tilde{\mathbf{Q}}_n^T$, $y_n^p = \tilde{\mathbf{Q}}_n y_n^q$, $\tilde{\mathbf{Q}}_n^T \tilde{\mathbf{Q}}_n = \mathbf{I}$,

$$\begin{aligned}
p(y_n^p | u) &\propto \exp \left(-\frac{1}{2} \left(y_n^p - \tilde{\mathbf{P}}_n \mathbf{P}_H u \right)^T \left(\tilde{\mathbf{P}}_n \mathbf{H}^\dagger \mathbf{R}(\mathbf{H}^\dagger)^T \tilde{\mathbf{P}}_n \right)^\dagger \left(y_n^p - \tilde{\mathbf{P}}_n \mathbf{P}_H u \right) \right) \\
&= \exp \left(-\frac{1}{2} \left(\tilde{\mathbf{Q}}_n (y_n^q - \tilde{\mathbf{Q}}_n^T \mathbf{P}_H u) \right)^T \left(\tilde{\mathbf{Q}}_n \tilde{\mathbf{Q}}_n^T \mathbf{H}^\dagger \mathbf{R}(\mathbf{H}^\dagger)^T \tilde{\mathbf{Q}}_n \tilde{\mathbf{Q}}_n^T \right)^\dagger \left(\tilde{\mathbf{Q}}_n (y_n^q - \tilde{\mathbf{Q}}_n^T \mathbf{P}_H u) \right) \right) \\
&= \exp \left(-\frac{1}{2} (y_n^q - \mathbf{H}_n^q u)^T \tilde{\mathbf{Q}}_n^T \tilde{\mathbf{Q}}_n (\mathbf{R}_n^q)^\dagger \tilde{\mathbf{Q}}_n^T \tilde{\mathbf{Q}}_n (y_n^q - \mathbf{H}_n^q u) \right) \\
&= \exp \left(-\frac{1}{2} (y_n^q - \mathbf{H}_n^q u)^T (\mathbf{R}_n^q)^\dagger (y_n^q - \mathbf{H}_n^q u) \right) \\
&= p(y_n^q | u) .
\end{aligned}$$

■

If in addition $p \leq M$ for $\tilde{\mathbf{P}}_n = \mathbf{P}_n$ or $0 < p + M - N \leq M$ for $\tilde{\mathbf{P}}_n = \mathbf{P}_n^H$, and $\mathbf{H} \tilde{\mathbf{Q}}_n$ is full rank, then the covariance matrix \mathbf{R}_n^q of y_n^q is invertible and y^q has a standard normal distribution. More generally for $(\mathbf{H}\mathbf{H}^T)^{-1}\mathbf{R}(\mathbf{H}\mathbf{H}^T)^{-1} = \mathbf{L}^T\mathbf{L}$, the Cholesky factorization, consider the SVD of $\mathbf{L}\mathbf{H}\mathbf{Q}_n = \mathbf{U}\Sigma\mathbf{V}^T$, then the rank of the covariance matrix $\mathbf{R}_n^q = \tilde{\mathbf{Q}}_n^T \mathbf{H}^\dagger \mathbf{R}(\mathbf{H}^\dagger)^T \tilde{\mathbf{Q}}_n = \mathbf{V}\Sigma^T\mathbf{V}^T$ is equal to the number of non-zero singular values of Σ .

Theorem 3.1 provides a blueprint for any DA scheme to be efficiently implemented with projected observations, involving the following changes: the observation y_n is replaced with y_n^q , the observation operator \mathbf{H} is replaced with \mathbf{H}_n^q , and the assumed measurement covariance \mathbf{R} is replaced with \mathbf{R}_n^q . This is only the most basic approach to using the projected data, and we will develop more complicated algorithms that use the orthogonal data, or even the original data, in addition to y_n^q .

A data model for the complementary orthogonal projection $\mathbf{I} - \tilde{\mathbf{P}}_n$ is easy to write down with 1.2. Define

$$(3.5) \quad y_n^{q\perp} = \left(\tilde{\mathbf{Q}}_n^\perp \right)^T \tilde{y}_n \in \mathbb{R}^{N-p} ,$$

where $\tilde{\mathbf{Q}}_n^\perp (\tilde{\mathbf{Q}}_n^\perp)^T = \mathbf{I} - \tilde{\mathbf{P}}_n$. The two projected data models are not independent in general and have joint distribution

$$(3.6) \quad \begin{bmatrix} y_n^q \\ y_n^{q\perp} \end{bmatrix} \sim \mathcal{N} \left(\begin{bmatrix} \mathbf{H}_n^q x_n^t \\ \mathbf{H}_n^{q\perp} x_n^t \end{bmatrix}, \begin{bmatrix} \mathbf{R}_n^q & \mathbf{R}_{12,n}^q \\ \mathbf{R}_{21,n}^q & \mathbf{R}_n^{q\perp} \end{bmatrix} \right) ,$$

where $\mathbf{H}^{q\perp} = (\tilde{\mathbf{Q}}_n^\perp)^T \mathbf{P}_H$, $\mathbf{R}^{q\perp} = (\tilde{\mathbf{Q}}_n^\perp)^T \mathbf{H}^\dagger \mathbf{R}(\mathbf{H}^\dagger)^T \tilde{\mathbf{Q}}_n^\perp$, and the off-diagonal covariances are $\mathbf{R}_{12,n}^q = \tilde{\mathbf{Q}}_n^T \mathbf{H}^\dagger \mathbf{R}(\mathbf{H}^\dagger)^T \tilde{\mathbf{Q}}_n^\perp$ and $\mathbf{R}_{21,n}^q = (\mathbf{R}_{12,n}^q)^T$.

4. Algorithms for Projected DA. In this section we discuss how some combination of the standard/projected forecast models (2.1), (1.1), (1.2) and data models (2.2), (3.4), (3.5)–(3.6) may be used to form a ‘projected DA scheme’.

A projected data model changes the innovation, the observation operator, and the observation error covariance. A projected physical model changes the prior and model error covariances. We want combinations of physical models, data models, and DA techniques that optimize the assimilation, particularly of the Particle Filtering schemes discussed in Section 2.2.

For comparison, past work on projected DA algorithms is now reviewed in the above framework. The standard AUS approach ([26], e.g.) can be derived by calculating the assimilation step using the projected model (1.1) and the original, unprojected data (2.2). This derivation will be performed in the next section. The projected shadowing approach of [8] iterates between assimilating unprojected data (2.2) into the projected model (1.1) and evolving the complementary orthogonal forecast model (1.2) without assimilation.

Neither AUS nor the shadowing approach have hitherto used projected data, though both may benefit from it. The use of projected data in AUS Particle Filters is a major topic for the remainder of the paper. For projected shadowing techniques, projected observations - that lie in the state space of the physical model - provide another means for generating an initial guess.

The DO-DA schemes in [35, 23, 27] use both a projected and mean field model to make a forecast, similar to using (1.1)–(1.2). The data is naturally split into the ‘projected’ and remaining components without using (3.4) explicitly, as the data may be confined to the DO-subspace by simply subtracting the forecast mean field. This attractive feature of the DO methodology bypasses the need to derive the projected data model (3.4), as the covariance structure of the data does not change.

We identify the following approaches to assimilating with projected data using the results of this paper:

Algorithm 1 (Project data only, and discard the orthogonal component). *Apply a standard DA scheme using the unprojected forecast model (2.1), but replace the standard data (2.2) with the projected data y_n^q of (3.4). The observation operator is replaced by \mathbf{H}_n^q , and the covariance matrix of the observations is replaced by \mathbf{R}_n^q .*

A Particle Filter employing Algorithm 1 will be tested on a stiff dissipative linear system in Section 5.1.

Algorithm 2 (Project model and data, discarding the orthogonal component of the data). *Apply a standard DA scheme, replacing the model with the projected component (1.1), and replacing the data with the projected component (3.4). Update the orthogonal component of the forecast using (1.2), without assimilation.*

The focus of this work is on projected data, and this algorithm will not be implemented here. However, it is mentioned as one approach to achieve a major reduction in the dimension of a DA problem, as both the model and data are projected. One problem-specific issue is that

the orthogonal component of the model is not corrected by any assimilation scheme and may introduce error; in [8] these errors were handled by iterating the update of the projected and unprojected model repeatedly.

Algorithm 3 (Project data and models, and assimilate both). *Project the forecast into the two subspaces, either by applying the projections $\tilde{\mathbf{P}}_n$ and $\mathbf{I} - \tilde{\mathbf{P}}_n$ to a forecast or by using the projected models (1.1)–(1.2). Apply a hybrid DA scheme that uses a method suitable for low-dimensional, nonlinear filtering to assimilate in the $\tilde{\mathbf{P}}_n$ -subspace, and a separate method suitable for high-dimensional filtering in the $(\mathbf{I} - \tilde{\mathbf{P}}_n)$ -subspace. When assimilating in the $\tilde{\mathbf{P}}_n$ -subspace use the corresponding data (3.4), and when assimilating in the orthogonal subspace use (3.5).*

The design of hybrid schemes such as the above is the subject of much interest lately; one such scheme is given by the DO-DA Blended PF [23]. Unlike the preceding or following schemes, the above description does not completely describe how to design such a hybrid DA scheme. The two DA schemes that assimilate in each subspace of Algorithm 3 must communicate information between each other, and should ideally respect the correlation of the two projected data models given in (3.6). (One can partially translate the DA algorithm between that paper and this: the state variables u_1 and u_2 there correspond to $\tilde{\mathbf{P}}_n u_n$ and $(\mathbf{I} - \tilde{\mathbf{P}}_n) u_n$ here, so the splitting in ([23], eqn. 1) of the prior density $p(u) = p(u_1)p(u_2|u_1)$ plays the same role as the projected models (1.1)–(1.2). The vectors \mathbf{e}_j in ([23], eqn. 8) are the columns of $\tilde{\mathbf{Q}}_n$ here. As mentioned above the DO formulation makes the two projected data models trivial to obtain, and their covariance structure in ([23], eqn. 15) is equivalent to the covariance described in (3.6).)

The last algorithm to be described is a novel, efficient PF scheme taking advantage of the Optimal Proposal PF described in section 2.2.1. The scheme differs from an Algorithm 1 implementation of OP-PF by using the full observations to form the proposal, and differs from an Algorithm 3 implementation by not using the orthogonal data $y_n^{q\perp}$ in the assimilation step.

Algorithm 4 (Blend projected and unprojected data in the assimilation step). *This algorithm describes a Particle Filter. For the particle update or proposal step, use the typical optimal proposal equations (2.8)–(2.9). Compute the weight update for each particle using the projected data model only, i.e. using an Algorithm 1 version of (2.10).*

Algorithm 4 uses all available data to update the particles, but only updates the weights based on how well the particles represent the projected data. This strategy will be tested on the chaotic Lorenz-96 system in Section 5.2. One major advantage of this approach is that it is requires no modification to the numerical simulation used to obtain the forecast. A second advantage is its efficiency; the full data are used for the particle update step, over which the update is straightforward and the dimension of the data does not lead to filter degeneracy; and only the projected data are used to avoid filter degeneracy in the weight update step. The scheme will prove to be more accurate than either, OP-PF or an Algorithm 1 implementation of OP-PF, in numerical tests.

4.1. Convergence results for projected algorithms. A normal line of inquiry for a new DA algorithm is to quantify the conditions under which it will well represent the posterior distribution, which neglecting time subscripts we write as $p(u|y)$. The projected algorithms above do not generally converge to $p(u|y)$, and so there are two questions: ‘Does the algorithm converge to a known distribution?’, and ‘How different is that distribution to the usual posterior?’.

Algorithm 1 clearly implements an approximation of the distribution $p(u|y^q)$, and similarly Algorithm 2 approximates $p(\tilde{\mathbf{P}}_n u|y^q)$. That is, a Particle Filter implementation of either approach would converge to the above distributions in the limit as the number of particles approaches infinity. The distribution approximated by Algorithm 3 is problem specific and may not be easy to write down, and similarly the distribution approximated by Algorithm 4 is a blending of $p(u|y)$ and $p(u|y^q)$ that is non-trivial to obtain in closed form.

We now quantify how the above distributions relate to the standard posterior $p(u_n|y_n)$. For this we will employ the Hellinger distance: given two probability distributions ρ and ρ' , with associated probability measures μ and μ' , the Hellinger distance between the two is

$$(4.1) \quad d_H(\mu, \mu') = \left[\frac{1}{2} \int \left(\sqrt{\rho(u)} - \sqrt{\rho'(u)} \right)^2 du \right]^{1/2}.$$

The Hellinger distance is a useful metric as it constrains the difference between functions in the two probability spaces, $|\mathbb{E}^\mu f(u) - \mathbb{E}^{\mu'} f(u)| \leq C d_H(\mu, \mu')$, true for any f that is square integrable over μ and μ' [20].

To bound this distance for Algorithm 1 we write $\rho(u) = p(u|y)$ and $\rho'(u) = p(u|y^q)$. The second distribution is written as

$$p(u|y^q) = p(u|y) \frac{p(y|y^q)}{p(y|u, y^q)},$$

obtained via Bayes’ law in the form $p(u) = p(u|y)p(y)/p(y|u)$, conditioning on y^q , and using $p(u|y, y^q) = p(u|y)$. Substituting into (4.1) we obtain a bound for the consistency of Algorithm 1 with the original posterior $p(u|y)$,

$$\begin{aligned} d_H(\mu, \mu') &= \left[\frac{1}{2} \int \left(1 - \sqrt{\frac{p(y|y^q)}{p(y|u, y^q)}} \right)^2 \rho(u) du \right]^{1/2} \\ &= \left[\frac{1}{2} \mathbb{E}^\mu \left(1 - \sqrt{\frac{p(y|y^q)}{p(y|u, y^q)}} \right)^2 \right]^{1/2}. \end{aligned}$$

Intuition on the projected algorithms suggests that if the projection somehow represents ‘important’ quantities in the model, e.g. directions associated with positive Lyapunov exponents, or coherent structures, etc, then the projected data will retain the same key information from the original data, and the posterior approximated by the projected DA algorithm will be similar to the original posterior. The above result quantifies that intuition. The posterior

distribution $p(u|y^q)$ associated with the projected algorithm will be close to $p(u|y)$ provided that the ratio $p(y|y^q)/p(y|u, y^q) \approx 1$ at the most likely values of u , that is, provided that the projected data contains information sufficient to constrain the values of the unprojected data in a neighbourhood of the truth. The ratio can be written as $p(y^{q\perp}|y^q)/p(y^{q\perp}|u, y^q)$ to further clarify that knowledge of the projected data should constrain the values of the orthogonal projected data.

A similar bound may easily be established for Algorithm 2. Let now $\rho'(u) = p(\tilde{\mathbf{P}}_n u|y^q)$, and μ' the associated probability measure; then

$$d_H(\mu, \mu') = \left[\frac{1}{2} \mathbb{E}^\mu \left(1 - \sqrt{\frac{p(\tilde{\mathbf{P}}_n u|y)}{p(u|y)} \frac{p(y|y^q)}{p(y|\tilde{\mathbf{P}}_n u, y^q)}} \right)^2 \right]^{1/2}.$$

The modification to this expression from the previous one is a second ratio that measures the information gap between the distribution of u and of $\tilde{\mathbf{P}}_n u$. As with the previous expression, the ratio is far from 1 if knowledge of $\tilde{\mathbf{P}}_n u$ does not constrain the possible values of $(\mathbf{I} - \tilde{\mathbf{P}}_n)u$ at all, and close to 1 if the projected data does have some relation to the full state.

An intuitive example of the above bounds in practice is a slow-fast system with a center manifold onto which the fast variables are attracted. Choosing $\tilde{\mathbf{P}}_n$ to identify the slow variables will lead to a small value of $d_H(\mu, \mu')$ for either Algorithm 1 or 2, since knowledge of the slow variables is sufficient to constrain the fast variables. In the case where there are few slow variables and many fast variables, then, an Algorithm 1 Particle Filter will be a much less degenerate implementation of the Particle Filter that converges close to the desired posterior $p(u|y)$. A linear system of this type will be the first numerical example, in Section 5.1.

5. Application: Assimilation in the Unstable Subspace. For the remainder of the paper we will study the case where the projection identifies the most unstable modes in the forecast model. To determine these modes we employ the discrete QR algorithm [9, 10]. For the discrete time model $u_{n+1} = F_n(u_n) + \omega_n$ with $u_n \in \mathbb{R}^N$, let $\mathbf{Q}_0 \in \mathbb{R}^{N \times p}$ ($p \leq N$) denote a random matrix such that $\mathbf{Q}_0^T \mathbf{Q}_0 = \mathbf{I}$,

$$(5.1) \quad \mathbf{Q}_{n+1} R_n = F'_n(u_n) \mathbf{Q}_n \approx \frac{1}{\epsilon} [F_n(u_n + \epsilon \mathbf{Q}_n) - F_n(u_n)], \quad n = 0, 1, \dots$$

where $\mathbf{Q}_{n+1}^T \mathbf{Q}_{n+1} = \mathbf{I}$ and R_n is upper triangular with positive diagonal elements. With a finite difference approximation the cost is that of an ensemble of size p plus a reduced QR via modified Gram-Schmidt to re-orthogonalize. Time dependent orthogonal projections to decompose state space are $\tilde{\mathbf{P}}_n = \tilde{\mathbf{Q}}_n \tilde{\mathbf{Q}}_n^T$ and $\mathbf{I} - \tilde{\mathbf{P}}_n = \mathbf{I} - \tilde{\mathbf{Q}}_n \tilde{\mathbf{Q}}_n^T$, where as described in Section 3.2 $\tilde{\mathbf{P}}_n$ refers either to \mathbf{P}_n or to the intersection of \mathbf{P}_n and \mathbf{P}_H .

In this section we establish the relationship between existing AUS algorithms and the projected data approach. For that reason, in this section AUS is used to refer only to traditional EKF-AUS ([37, 26], e.g.). This approach implements a modified EKF in which the forecast covariance matrix P_n^f is replaced by the projected matrix $\mathbf{P}_n P_n^f \mathbf{P}_n$, leading to the Kalman

gain

$$(5.2) \quad \mathbf{K}_n = \mathbf{P}_n P_n^f \mathbf{P}_n \mathbf{H}^T \left[\mathbf{H} \mathbf{P}_n P_n^f \mathbf{P}_n \mathbf{H}^T + \mathbf{R} \right]^{-1},$$

where the EKF forecast covariance matrix P_n^f and observation operator \mathbf{H} are described in Section 2.1.1. It is clear that the EKF-AUS Kalman gain can be written as a combination of the columns of \mathbf{Q}_n .

The Algorithm 1 implementation of the EKF, with projection $\tilde{\mathbf{P}}_n \equiv \mathbf{P}_n$ to compare with AUS, would have Kalman gain given by

$$(5.3) \quad \mathbf{K}_n = P_n^f \mathbf{P}_n \mathbf{H} \mathbf{P}_n \left[\mathbf{P}_n \mathbf{H}^\dagger \left(\mathbf{H} P_n^f \mathbf{H}^T + \mathbf{R} \right) (\mathbf{H}^\dagger)^T \mathbf{P}_n \right]^\dagger.$$

The difference between the two Kalman gains is essentially that (5.3) interchanges the position of \mathbf{H} and \mathbf{P}_n , requiring the use of \mathbf{H}^\dagger in order to do so, but manages to project all terms in the covariance-weighting inverse instead of only the forecast covariance matrix. Unlike the classical AUS gain (5.2), (5.3) does not restrict the analysis increment to the unstable subspace. The innovation is $y_n - \mathbf{H} u_n^f$ in classical AUS, but with (5.3) would be $y_n^q - \mathbf{P}_n \mathbf{P}_n \mathbf{H} u_n^f$.

That is, classical AUS uses the full data but restricts the assimilation update to the unstable subspace via (5.2); Algorithm 1 restricts the innovation to the unstable subspace but the assimilation update can distribute this innovation across the whole of model space. The comparison between these algorithms here is pedagogical, not competitive; the advantages of the EKF-AUS algorithm are well established, while Algorithm 1 effects a reduction in data dimension that we will explore for Particle Filters, not the EKF.

Finally we obtain a form of EKF associated with the projected models (1.1)–(1.2) and unprojected data. This is essentially a re-derivation of EKF-AUS from the projected framework employed in this paper, confirming that the two are compatible. Consider the linearized physical model $u_{n+1} = \mathbf{A}_n u_n + \omega_n$ of Section 2.1.1. Then the projected physical model has the form $\tilde{\mathbf{P}}_{n+1} u_{n+1} = \tilde{\mathbf{P}}_{n+1} \mathbf{A}_n \tilde{\mathbf{P}}_n u_n + \tilde{\mathbf{P}}_{n+1} \omega_n$ or

$$\begin{aligned} v_{n+1} &= \tilde{\mathbf{P}}_{n+1} u_{n+1} = [\tilde{\mathbf{Q}}_{n+1} R_n \tilde{\mathbf{Q}}_n^T] v_n + \tilde{\mathbf{P}}_{n+1} \omega_n \\ &\equiv \mathbf{B}_n v_n + \tilde{\mathbf{P}}_{n+1} \omega_n, \end{aligned}$$

where $v_n = \tilde{\mathbf{P}}_n u_n$ and using $\tilde{\mathbf{P}}_{n+1} \mathbf{A}_n \tilde{\mathbf{P}}_n = \tilde{\mathbf{Q}}_{n+1} R_n \tilde{\mathbf{Q}}_n^T$. The forecast covariance matrix is

$$\begin{aligned} \tilde{P}_{n+1}^f &= \tilde{\mathbf{P}}_{n+1} \mathbf{A}_n \tilde{P}_n^a \mathbf{A}_n^T \tilde{\mathbf{P}}_{n+1} + \tilde{\mathbf{P}}_{n+1} \Sigma \tilde{\mathbf{P}}_{n+1} \\ &= \mathbf{A}_n (\tilde{\mathbf{P}}_n \tilde{P}_n^a \tilde{\mathbf{P}}_n) \mathbf{A}_n^T + \tilde{\mathbf{P}}_{n+1} \Sigma \tilde{\mathbf{P}}_{n+1} \end{aligned}$$

since $\mathbf{B}_n = \mathbf{A}_n \tilde{\mathbf{P}}_n$. The first row of the forecast covariance matrix is the EKF-AUS forecast covariance if $\tilde{P}_n^a = P_n^a$ and $\tilde{\mathbf{P}}_n = \mathbf{P}_n$, and so the assimilation step produces EKF-AUS with Kalman gain (5.2).

We will now explore the benefits of the projected data algorithms in an AUS framework. For the remainder of the paper we refer to the projected DA schemes as AUS schemes, e.g. PF-AUS for an Algorithm 1 Particle Filter and OP-PF-AUS for an Algorithm 4 Optimal Proposal Particle Filter.

The first test case is a simple linear model that demonstrates the situation in which PF-AUS will significantly improve on the standard Particle Filter.

5.1. Case study: linear model with Gaussian noise. Suppose that forecasts are made with a physical model of the form

$$\frac{du}{dt} = \mathbf{A}u + \sigma \dot{W},$$

where W is a Wiener process. The one-step model (2.1) is obtained through a simulation of this physical model with a standard numerical integrator, initialised at one observation time and terminating at the next. We construct \mathbf{A} so that it has two eigenvalues with small real part $Re(\lambda_i) \in (0, 0.04)$, and so that the remaining 98 eigenvalues have real part $Re(\lambda_i) \leq -100$. This produces a well known multiscale dynamic, which we describe for the deterministic case $\sigma = 0$. There exists a transformation of this system into a system consisting of 2 ‘slow’ and 98 ‘fast’ variables. The fast variables are rapidly attracted onto a slow invariant manifold that depends only on the slow variables. Using centre manifold theory [6] one can obtain an expression for this slow manifold, and furthermore calculate an ordinary differential equation that governs the evolution of the 2 slow variables.

We run DA experiments assuming that the slow manifold and reduced system are unknown, instead using forecasts and observations from the full, 100-dimensional system. The key to a successful assimilation step will be to get the correct distribution for the (unknown) 2-dimensional subspace of model space corresponding to the slow variables.

We present results for the PF compared to PF-AUS using Algorithm 1. Four scenarios are considered: where every variable is observed, every second variable, every fourth variable, and finally a scenario in which only two variables are observed. We collect these observations every 0.1 time units until 100 observation times have passed, with small measurement error covariance $\mathbf{R} = 0.05^2 \mathbf{I}$ and model noise $\sigma = 0.05$. Both PF algorithms resample if the ESS drops below half the number of particles, which is 1000. On resampling, noise is added to every variable with a standard deviation of 0.02. We use PF-AUS with $p = 2$.

We report the RMSE between the filter mean at each time step and the true system state. The standard Particle Filter performs very poorly with high dimensional data, while PF-AUS is reasonably indifferent to the dimension of the data and in all cases has mean RMSE below the RMSE of the observations. Results are displayed in Figure 1.

Two extremes of the data dimension serve to highlight its role in Particle Filter divergence. In Figure 1a every variable is accurately observed, and consequently one could obtain a reasonable estimate of the system at every observation time by directly using the data. Despite this, and despite the low-dimensional attractor in the state dynamics, the Particle Filter estimate diverges frequently and far from the true state. The other extreme in data availability is

Figure 1d, in which only two variables are observed and the Particle Filter has an accurate mean RMSE of 0.03. By comparison PF-AUS is more accurate than the observations in each scenario, and in particular does not diverge at large data dimension.

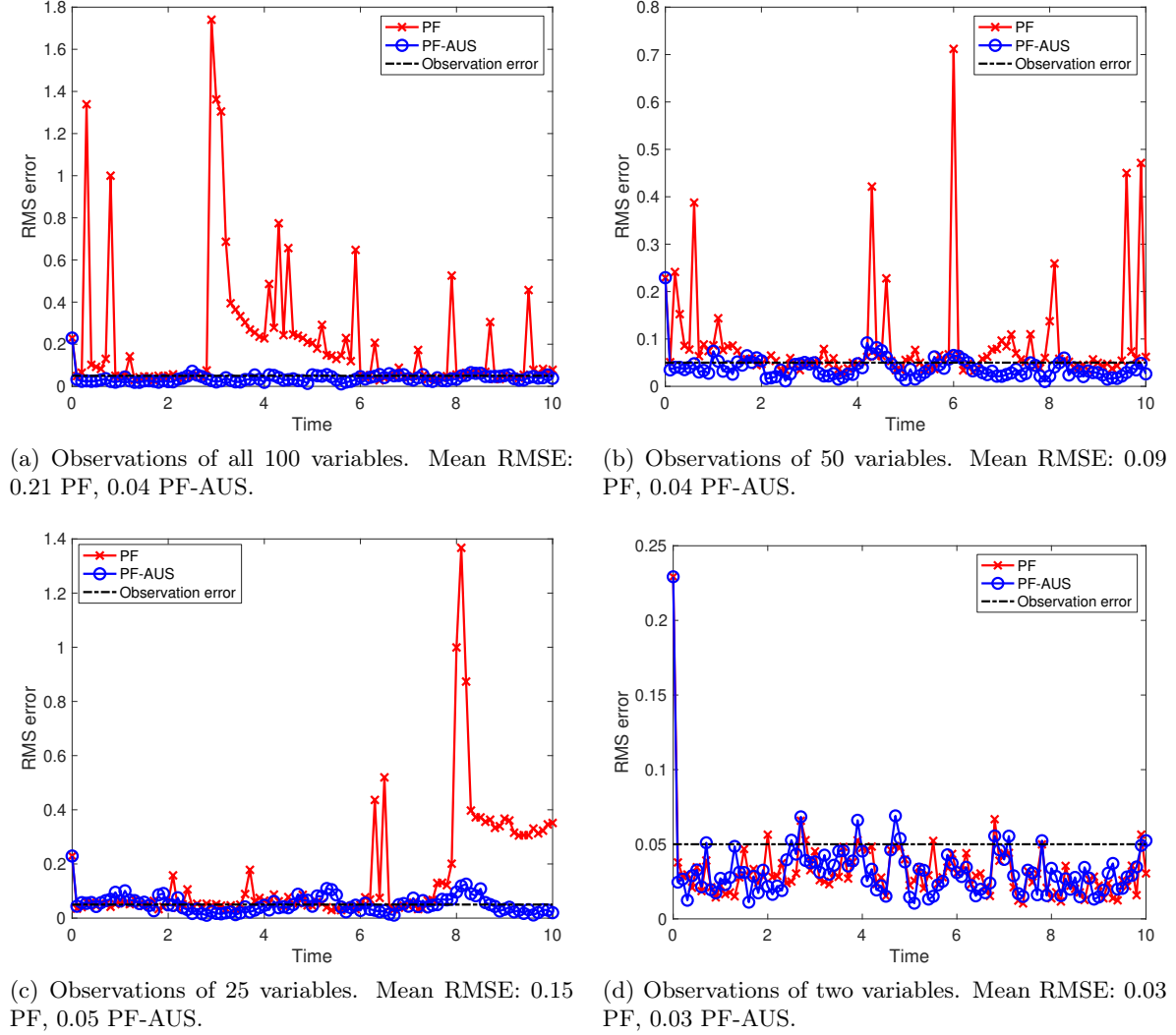


Figure 1: Comparison of the Particle Filter to an Algorithm 1 implementation of PF-AUS for a linear system as the number of variables observed is changed.

We now present examples from the Lorenz 96 system.

5.2. Case Study: Chaotic Lorenz 96 system. Consider the system of ordinary differential equations introduced in [21],

$$(5.4) \quad \dot{x}_i = (x_{i+1} - x_{i-2}) x_{i-1} - x + F, \quad$$

where i runs from 1 to J , and $F = 8$. If $J = 40$, then this system is chaotic with 14 positive and 1 neutral Lyapunov exponents.

We present experiments in which the deterministic part of the model (2.1) is given by an integration of (5.4) for a fixed time.

In this section we will implement Algorithm 4, OP-PF-AUS, and compare to the OP-PF and EnKF. We make the following modification to resampling in OP-PF-AUS:

Algorithm 5 (Resampling in the Unstable Subspace). *When adding noise after resampling, generate (the usual) noise sampled from $\mathcal{N}(\mathbf{0}, \omega^2 \mathbf{I})$, and then multiply this random vector by $\alpha \tilde{\mathbf{P}}_n + (1 - \alpha)I$, for some $\alpha \in [0, 1]$.*

When $\alpha = 0$ this algorithm is no different to the normal resampling approach, but for $\alpha > 0$ some proportion of the uncertainty in resampling is constrained to lie in the space spanned by the columns of $\tilde{\mathbf{Q}}_n$. For AUS the resampling scheme should add more noise in the directions of greatest uncertainty in the forecast model, which provides one advantage; a second advantage is that the algorithm does not shift particles as far off the attractor.

We now tune α in Algorithm 5 to demonstrate the benefit of constraining resampling noise to the most unstable directions. For this experiment the mean RMSE and percentage of resampling steps were recorded for 20 runs of OP-PF-AUS at 20 different values of ω and 10 different values of α , choosing $p = 3$ for OP-PF-AUS. Figure 2 clearly displays that the RMSE and filter degeneracy both strictly decrease as α increases, at all considered values of ω . For this experiment the model noise covariance is $\Sigma = 0.01\mathbf{I}$, and every second variable is observed with error covariance $\mathbf{R} = 0.01\mathbf{I}$.

The remaining experiments use Algorithm 5 for resampling in the AUS algorithms with $\alpha = 0.99$. The resampling noise ω is optimised separately in the standard PF and the PF-AUS algorithms by choosing the minimum RMSE result over 20 values in $[10^{-4}, 10^{-2}]$.

We now investigate the optimal choice of dimension p for the projected data in OP-PF-AUS. One might expect that $p \geq 15$ would be optimal, as the system has 15 unstable and neutral modes. However, the blending of projected and unprojected data in Algorithm 4 will sufficiently constrain the weakly unstable modes in the system, and at the same time the PF algorithm will avoid degeneracy at low values of p . The RMSE and number of resampling steps taken by OP-PF-AUS compared to OP-PF are displayed in Figure 3. The RMSE has a clear minimum at $p = 6$, about 30% less than the OP-PF RMSE, and the frequency of resampling in OP-PF-AUS decreases sharply with p . The optimal choice of noise to add on resampling was $\omega = 0.0027$ for OP-PF, and $\omega = 0.056$ for OP-PF-AUS. The optimal noise for OP-PF-AUS is an order of magnitude larger than for OP-PF. This suggests that one benefit of the novel resampling scheme is the ability to more vigorously explore the uncertain directions in the forecast without moving system estimates too far off any local attractor.

The selection of p in a non-degenerate DA scheme is less crucial. For comparison to Figure 3 we implement an ETKF and compare to ETKF-AUS (implemented via the projected data approach of Algorithm 1). The same experimental parameters are used as for the PF results, except for the ensemble size which is 50. Results are shown in Figure 4. For the EnKF-AUS

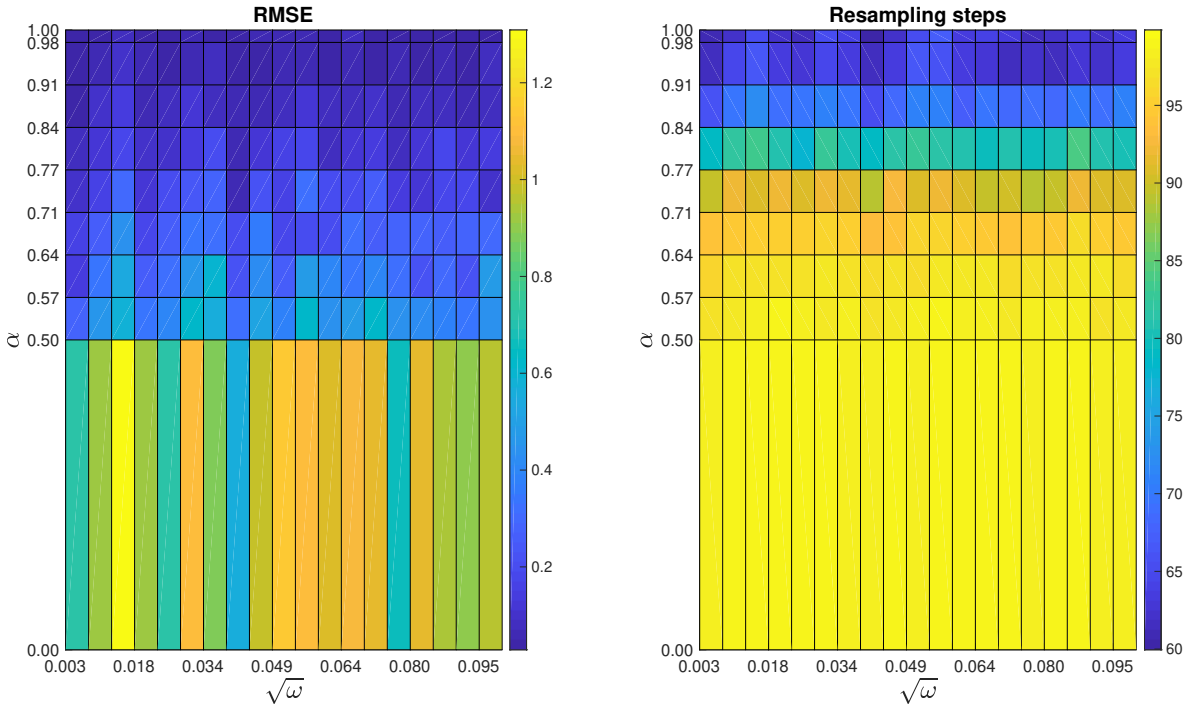


Figure 2: Statistics for the resampling scheme Algorithm 5 as the resampling noise ω and confinement to the unstable subspace α are varied for the Lorenz96 system. Data points are the vertices of the shaded surface, and the shading in each cell reflects the trend across all 4 vertices. Each data point represents the mean from 20 repetitions, each of which was also time-averaged.

Left: RMSE (with value given in color bar). Increasing α uniformly improves the error. *Right:* percentage of assimilation steps that trigger resampling (value shown in color bar). Increasing α decreases the phenomenon of resampling, that is it mitigates filter degeneracy.

the error statistics are similar for a large range $5 \leq p \leq 13$, about 20% below the mean ETKF behaviour¹.

The above experiments all took place in parameter regimes in which OP-PF was quite accurate (if degenerate). We now turn to parameter regimes that are difficult for the Optimal Proposal. In particular we choose moderate model noise with $\Sigma = (0.3)^2 \mathbf{I}$ and large measurement error $\mathbf{R} = 1\mathbf{I}$. We also initialise each method with a tight ensemble spread of standard deviation 0.01

¹It is a little surprising that the ETKF-AUS does any better than ETKF at all, as the ETKF does not suffer from the curse of dimensionality. An Algorithm 1 implementation of the Kalman Filter does not improve on the standard KF, so it is a detail of implementation and not of fundamental structure that ETKF-AUS has lower mean RMSE than ETKF. It may be that the dimension reduction involved in ETKF-AUS ameliorates ill-conditioning in the inverse of the Kalman gain in such a manner that the ETKF is thereby improved; but if so the mechanism of improvement is still not clear, since the ETKF was designed for exactly that scenario already [15].

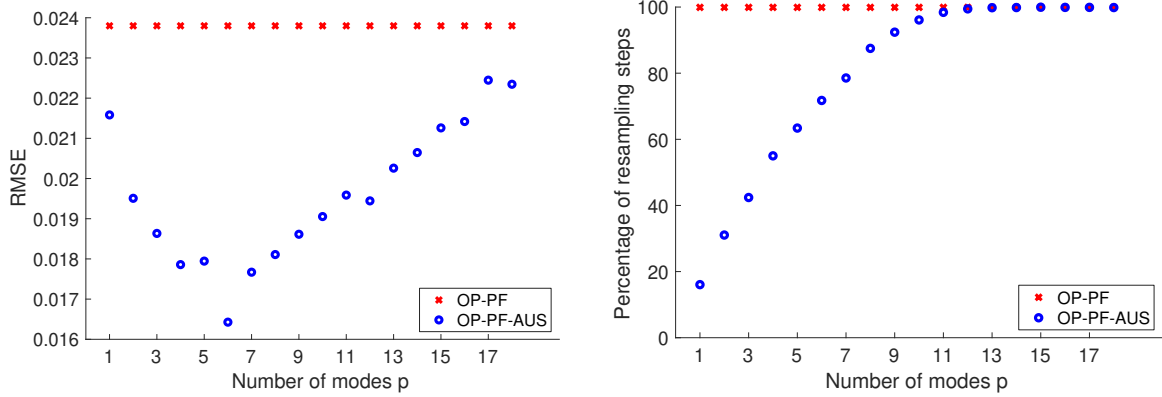


Figure 3: Tuning OP-PF-AUS as the rank of the projection is varied, compared to the Optimal Proposal PF, for the Lorenz96 system in a configuration when the Optimal Proposal performs well. Each data point represents the mean from 20 repetitions, each of which was also time-averaged.

around a strongly biased initial condition, with initial RMSE of 1.5. Figure 5 clearly displays the advantage of OP-PF-AUS over OP-PF in this regime. The optimal choice of $p = 2$ has about 60% lower RMSE than OP-PF and is not degenerate, resampling only on 30% of steps (compared to 99.5% of steps for OP-PF). For comparison, we plot one realization of OP-PF and of the LETKF (localised to 12 variables and with inflation 1.02) against OP-PF-AUS with $p = 2$ in Figure 6. The OP-PF-AUS is the best scheme of the three with these experimental parameters, though in general the EnKF is a stable and accurate scheme for the Lorenz 96 system. We emphasise that in general the LETKF will have lower RMSE than OP-PF-AUS; one would expect to see benefits from the Particle Filter-derived scheme in representing a multimodal, or otherwise less Gaussian, posterior.

Finally, we investigate the behaviour of OP-PF-AUS as the dimension J of the Lorenz96 system is varied from 40 to 400. We use accurate model covariance $\Sigma = 0.04^2\mathbf{I}$ and observation covariance $\mathbf{R} = 0.01^2\mathbf{I}$. We choose to project onto the $p = 8$ most unstable modes for OP-PF-AUS, and use as a benchmark results from an ETKF. Results for this scenario are displayed in Figure 1. We see the OP-PF diverge, while OP-PF-AUS performs almost as well as the Ensemble Kalman Filter.

6. Discussion. In this work a new approach to DA has been derived that allows for dimension reduction of the data using a projection defined in state space. The chief application has been Particle Filters Assimilating in the Unstable Subspace, which the classical AUS approach is unsuitable for because ensemble methods already project the forecast strongly into the unstable subspace [3] and because the classical AUS approach does not greatly change the weight update, the cause of filter degeneracy. By contrast the new approach sharply reduces filter degeneracy in a predictable fashion, improves filter accuracy and allows one to construct

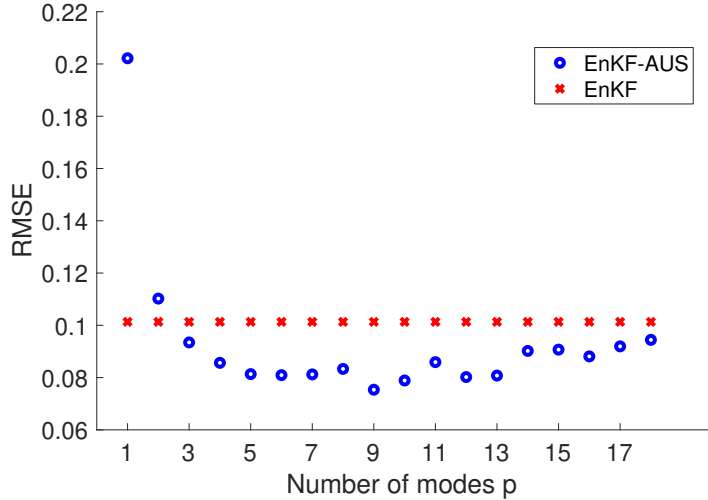


Figure 4: Statistics for EnKF-AUS as the rank of the projection is varied, compared to the Ensemble Kalman Filter, for the Lorenz96 system. Each data point represents the mean from 20 repetitions, each of which was also time-averaged. Somewhat surprisingly, projecting the data reduces the error in the EnKF for this experiment, though to a lesser extent than for the PF methods.

a sensible resampling scheme that adds more noise in more uncertain directions. Algorithms resting on the projected DA approach were tested on a sample linear system to investigate the role of data dimension in a simple context, and on the chaotic Lorenz 96 system that provides a challenging scenario for particle filters. The projected DA approach was also found to have some benefits for the Ensemble Kalman Filter.

Two algorithms were tested; the first allows the projected DA formulation to be simply applied to any DA scheme, while the second is a particle filter that mixes projected and unprojected data based on the optimal proposal.

Existing work in AUS and in data-driven algorithms employing projections suggest some improvements that will drive further work in this area. The discrete QR technique used to find the unstable subspace in this work is rigorously justified and the cost is proportional to employing an ensemble size of the dimension of the unstable subspace. A related branch of work in [23] used both the projected and orthogonal data sets, and the extension of those algorithms to the general projected DA case is of interest. The projected shadowing scheme [8] used iteration to improve the analysis of the projected and orthogonal models, and developing an iteration scheme in this framework is one way to correct the projections to include information that is present in the data but absent in the model. Finally, some projection-based DA schemes have been developed to assimilate coherent structures [22] or features [24] in the data. These approaches have used likelihood-free sequential monte carlo methods, or an ad hoc ‘perturbed observations’ approach, to deal with the difficulty of calculating the likelihood function for a coherent structure. The derivation in this paper may lead to an explicit likelihood for data-derived coherent structures/features obtained via a projection.

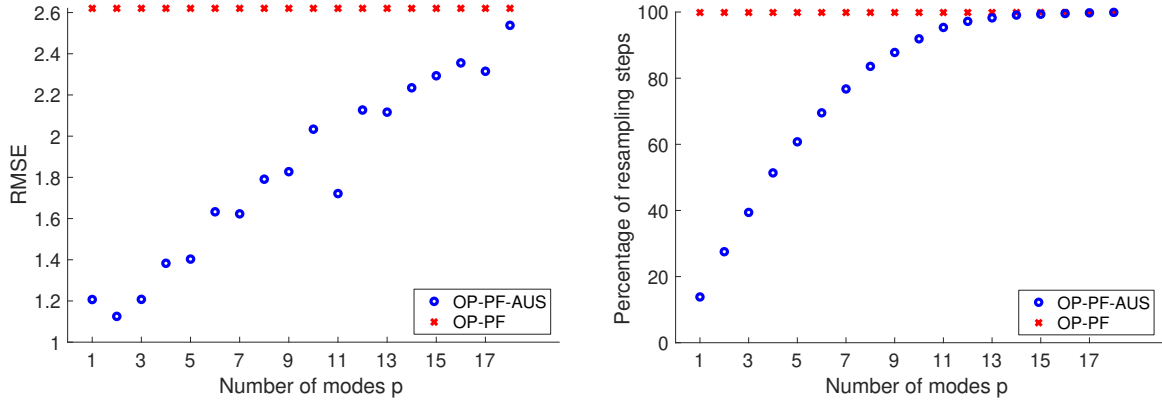


Figure 5: Statistics for OP-PF-AUS as the rank of the projection is varied, compared to the Optimal Proposal PF, for the Lorenz96 system in a configuration where the Optimal Proposal performs poorly. Each data point represents the mean from 20 repetitions, each of which was also time-averaged.

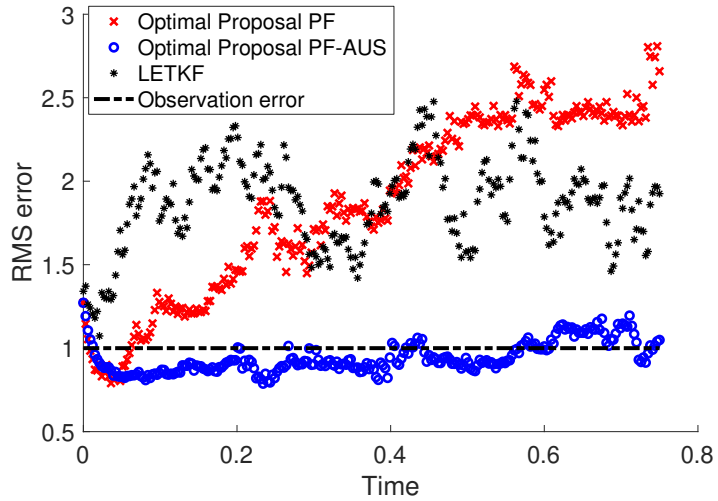


Figure 6: Error statistics for the DA methods over time, from one of the realizations of Figure 5 with $p = 2$.

Acknowledgements. JM acknowledges the support of ONR grant N00014-18-1-2204, NSF grant DMS-1722578, and the Australian Research Council Discovery Project DP180100050. EVV acknowledges the support of NSF grants DMS-1714195 and DMS-1722578. The authors are grateful to Alberto Carrassi for helpful feedback on an early version of this work.

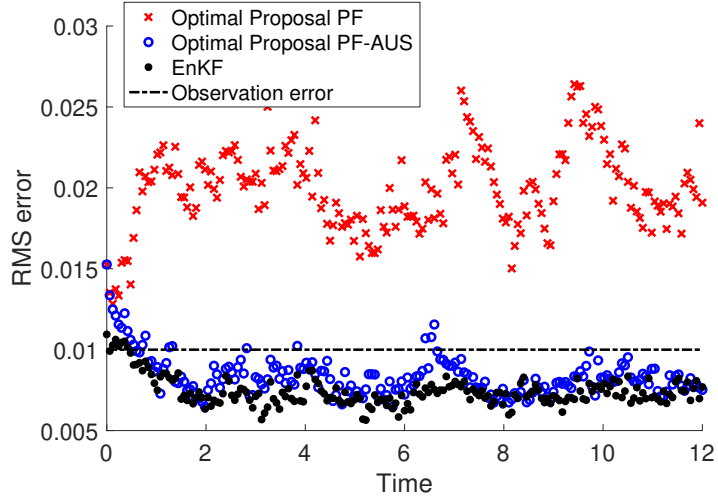


Figure 7: Error statistics for the DA methods over time, from the 400-dimensional Lorenz96 system with accurate observations of every second variable. In this case the ETKF is used to provide a ‘good performance’ benchmark for OP-PF-AUS.

Appendix A. Projections onto convex sets. Given two orthogonal projections $\mathbf{P}_A, \mathbf{P}_B$, the following algorithms identify the projection $\mathbf{P}_{A \cap B}$.

Von Neumann’s algorithm iterates the product of the projections,

$$\mathbf{P}_{A \cap B} = \lim_{k \rightarrow \infty} (\mathbf{P}_A \mathbf{P}_B)^k$$

Dykstra’s projection algorithm generally converges faster.

Start with $x_0 = \mathbf{I}$, $p_0 = q_0 = k = 0$, and update by

$$\begin{aligned} y_k &= \mathbf{P}_A(x_k + p_k) \\ p_{k+1} &= x_k + p_k - y_k \\ x_{k+1} &= \mathbf{P}_B(y_k + q_k) \\ q_{k+1} &= y_k + q_k - x_{k+1}. \end{aligned}$$

Then $\mathbf{P}_{A \cap B} = \lim_{k \rightarrow \infty} x_k$.

Either algorithm may be used with some tolerance on the change in the approximation of $\mathbf{P}_{A \cap B}$, or to some finite k .

REFERENCES

- [1] M. ASCH, M. BOCQUET, AND M. NODET, *Data assimilation: methods, algorithms, and applications*, vol. 11, SIAM, 2016.
- [2] C. H. BISHOP, B. J. ETHERTON, AND S. J. MAJUMDAR, *Adaptive sampling with the ensemble transform Kalman filter. Part I: Theoretical aspects*, Monthly weather review, 129 (2001), pp. 420–436.

[3] M. BOCQUET AND A. CARRASSI, *Four-dimensional ensemble variational data assimilation and the unstable subspace*, Tellus A: Dynamic Meteorology and Oceanography, 69 (2017), p. 1304504.

[4] A. BUDHIRAJA, E. FRIEDLANDER, C. GUIDER, C. K. JONES, AND J. MACLEAN, *Data assimilation; inference for linking physical and probabilistic models for complex nonlinear dynamic systems*, in Handbook of Environmental and Ecological Statistics, A. E. Gelfand, M. Fuentes, J. A. Hoeting, and R. L. Smith, eds., CRC Press, 1 ed., 9 2017, pp. 687–708.

[5] G. BURGERS, P. JAN VAN LEEUWEN, AND G. EVENSEN, *Analysis scheme in the ensemble Kalman filter*, Monthly weather review, 126 (1998), pp. 1719–1724.

[6] J. CARR, *Applications of centre manifold theory*, vol. 35, Springer Science & Business Media, 2012.

[7] A. CARRASSI, M. GHIL, A. TREVISAN, AND F. UBOLDI, *Data assimilation as a nonlinear dynamical systems problem: Stability and convergence of the prediction-assimilation system*, Chaos, 18 (2008), p. 023112.

[8] B. DE LEEUW, S. DUBINKINA, J. FRANK, A. STEYER, X. TU, AND E. VAN VLECK, *Projected shadowing-based data assimilation*, SIAM Appld. Dyn. Sys., (2018).

[9] L. DIECI AND E. S. VAN VLECK, *Lyapunov and Sacker-Sell spectral intervals*, J. Dynam. Differential Equations, 19 (2007), pp. 265–293, <https://doi.org/10.1007/s10884-006-9030-5>, <https://doi.org/www2.lib.ku.edu/10.1007/s10884-006-9030-5>.

[10] L. DIECI AND E. S. VAN VLECK, *Lyapunov exponents: Computation*, in Encyclopedia of Applied and Computational Mathematics, B. Engquist, ed., Springer-Verlag, 2015.

[11] A. DOUCET, N. DE FREITAS, AND N. GORDON, *An introduction to sequential Monte Carlo methods*, in Sequential Monte Carlo methods in practice, A. Doucet, N. De Freitas, and N. Gordon, eds., Springer, 2001, pp. 3–14.

[12] A. DOUCET, S. GODSILL, AND C. ANDRIEU, *On sequential Monte Carlo sampling methods for Bayesian filtering*, Statistics and computing, 10 (2000), pp. 197–208.

[13] G. EVENSEN, *Sequential data assimilation with a nonlinear quasi-geostrophic model using Monte Carlo methods to forecast error statistics*, Journal of Geophysical Research: Oceans, 99 (1994), pp. 10143–10162.

[14] G. EVENSEN, *Data assimilation: the ensemble Kalman filter*, Springer Science & Business Media, 2009.

[15] G. EVENSEN AND P. J. VAN LEEUWEN, *Assimilation of Geosat altimeter data for the Agulhas current using the ensemble kalman filter with a quasigeostrophic model*, Monthly Weather Review, 124 (1996), pp. 85–96.

[16] C. GONZÁLEZ-TOKMAN AND B. R. HUNT, *Ensemble data assimilation for hyperbolic systems*, Physica D: Nonlinear Phenomena, 243 (2013), pp. 128–142.

[17] B. R. HUNT, E. J. KOSTELICH, AND I. SZUNYOGH, *Efficient data assimilation for spatiotemporal chaos: A local ensemble transform Kalman filter*, Physica D: Nonlinear Phenomena, 230 (2007), pp. 112–126.

[18] E. KALNAY, *Atmospheric modeling, data assimilation and predictability*, Cambridge university press, 2003.

[19] K. LAW, D. SANZ-ALONSO, A. SHUKLA, AND A. STUART, *Controlling unpredictability with observations in the partially observed Lorenz '96 model*, ArXiv e-prints, (2014), <https://arxiv.org/abs/1411.3113>.

[20] K. LAW, A. STUART, AND Z. KONSTANTINOS, *Data Assimilation: A Mathematical Introduction*, vol. 62, Springer Texts in Applied Mathematics, 2015.

[21] E. N. LORENZ, *Predictability - a problem partly solved*, in Proceedings of seminar on Predictability, T. Palmer and R. Hagedorn, eds., vol. 1, Reading, UK, 1996, ECMWF, Cambridge University Press, pp. 1–18.

[22] J. MACLEAN, N. SANTITISSADEEKORN, AND C. K. R. T. JONES, *A coherent structure approach for parameter estimation in Lagrangian data assimilation*, Phys. D, 360 (2017), pp. 36–45, <https://doi.org/10.1016/j.physd.2017.08.007>, <https://doi.org/www2.lib.ku.edu/10.1016/j.physd.2017.08.007>.

[23] A. J. MAJDA, D. QI, AND T. P. SAPSIS, *Blended particle filters for large-dimensional chaotic dynamical systems*, Proc. Natl. Acad. Sci. USA, 111 (2014), pp. 7511–7516, <https://doi.org/10.1073/pnas.1405675111>, <https://doi.org/www2.lib.ku.edu/10.1073/pnas.1405675111>.

[24] M. MORZFIELD, J. ADAMS, S. LUNDERMAN, AND R. OROZCO, *Feature-based data assimilation in geophysics*, Nonlinear Processes in Geophysics, 25 (2018), pp. 355–374.

[25] M. MORZFIELD, X. TU, E. ATKINS, AND A. J. CHORIN, *A random map implementation of implicit filters*, J. Comput. Phys., 231 (2012), pp. 2049–2066, <https://doi.org/10.1016/j.jcp.2011.11.022>, <https://doi.org/www2.lib.ku.edu/10.1016/j.jcp.2011.11.022>.

//doi.org.www2.lib.ku.edu/10.1016/j.jcp.2011.11.022.

- [26] L. PALATELLA, A. CARRASSI, AND A. TREVISAN, *Lyapunov vectors and assimilation in the unstable subspace: theory and applications*, Journal of Physics A: Mathematical and Theoretical, 46 (2013), p. 254020, <http://stacks.iop.org/1751-8121/46/i=25/a=254020>.
- [27] D. QI AND A. J. MAJDA, *Blended particle methods with adaptive subspaces for filtering turbulent dynamical systems*, Phys. D, 298/299 (2015), pp. 21–41, <https://doi.org/10.1016/j.physd.2015.02.002>, <https://doi.org.www2.lib.ku.edu/10.1016/j.physd.2015.02.002>.
- [28] S. REICH AND C. COTTER, *Probabilistic forecasting and Bayesian data assimilation*, Cambridge University Press, 2015.
- [29] D. SANZ-ALONSO AND A. M. STUART, *Long-time asymptotics of the filtering distribution for partially observed chaotic dynamical systems*, SIAM/ASA Journal on Uncertainty Quantification, 3 (2015), pp. 1200–1220, <https://doi.org/10.1137/140997336>.
- [30] T. SAPSIS, *Dynamically orthogonal field equations*, PhD thesis, Massachusetts Institute of Technology, Department of Mechanical Engineering, 2010.
- [31] T. P. SAPSIS AND P. F. J. LERMUSIAUX, *Dynamically orthogonal field equations for continuous stochastic dynamical systems*, Phys. D, 238 (2009), pp. 2347–2360, <https://doi.org/10.1016/j.physd.2009.09.017>, <https://doi.org.www2.lib.ku.edu/10.1016/j.physd.2009.09.017>.
- [32] C. SNYDER, *Particle filters, the "optimal" proposal and high-dimensional systems*, in Proceedings of the ECMWF Seminar on Data Assimilation for atmosphere and ocean, 2011, pp. 1–10.
- [33] C. SNYDER, T. BENGSSON, P. BICKEL, AND J. ANDERSON, *Obstacles to high-dimensional particle filtering*, Monthly Weather Review, 136 (2008), pp. 4629–4640.
- [34] C. SNYDER, T. BENGSSON, AND M. MORZFIELD, *Performance bounds for particle filters using the optimal proposal*, Monthly Weather Review, 143 (2015), pp. 4750–4761.
- [35] T. SONDERGAARD AND P. F. LERMUSIAUX, *Data assimilation with Gaussian mixture models using the dynamically orthogonal field equations. Part I: Theory and scheme*, Monthly Weather Review, 141 (2013), pp. 1737–1760.
- [36] A. TREVISAN, M. D'ISIDORO, AND O. TALAGRAND, *Four-dimensional variational assimilation in the unstable subspace and the optimal subspace dimension*, Q.J.R. Meteorol. Soc., 136 (2010), pp. 487–496, <https://doi.org/10.1002/qj.571>.
- [37] A. TREVISAN AND L. PALATELLA, *On the Kalman filter error covariance collapse into the unstable subspace*, Nonlinear Processes in Geophysics, 18 (2011), pp. 243–250.
- [38] H. TSUKUMA AND T. KUBOKAWA, *Estimation of the mean vector in a singular multivariate normal distribution*, J. Multivariate Anal., 140 (2015), pp. 245–258, <https://doi.org/10.1016/j.jmva.2015.05.016>, <https://doi.org.www2.lib.ku.edu/10.1016/j.jmva.2015.05.016>.
- [39] P. VAN LEEUWEN, *Particle filters for the geosciences*, Advanced Data Assimilation for Geosciences: Lecture Notes of the Les Houches School of Physics: Special Issue, (2012), p. 291.
- [40] P. J. VAN LEEUWEN, *Nonlinear data assimilation in geosciences: an extremely efficient particle filter*, Quarterly Journal of the Royal Meteorological Society, 136 (2010), pp. 1991–1999.
- [41] P. J. VAN LEEUWEN, H. R. KÜNSCH, L. NERGER, R. POTTHAST, AND S. REICH, *Particle filters for applications in geosciences*, arXiv preprint arXiv:1807.10434, (2018).